CALCULATIONS OF EM INTERACTIONS WITH BIOLOGICAL TISSUE: MAGNETIC RESONANCE IMAGING AT ULTRA HIGH FIELD

Tamer S. Ibrahim[*#], Robert Lee[^#], Brian A. Baertlein[#]
Amir Abduljalil[*], and Pierre-Marie L. Robitaille[*]

Departments of Radiology[*] and Electrical Engineering[#]
The Ohio State University, Columbus, Ohio 43210

[^] *Address correspondence to:*
Robert Lee or Pierre-Marie Robitaille
The Ohio State University
Department of Electrical Engineering
2015 Neil Avenue
Columbus, OH 43210
E-mail address: lee@ee.eng.ohio-state.edu

ABSTRACT

A finite difference time domain model is developed to simulate a TEM resonator for high frequency clinical magnetic resonance imaging applications. The coil-head electromagnetic interactions and their effects on the SAR in biological tissue are presented. The TEM resonator and the newly developed 18-tissue anatomically detailed human head model are treated together as a single system. This is done through all the steps of the model including excitation and numerical tuning. The treatment of the resonator and the head as a single system and the geometrical modeling of all the coil components including coaxial rods, shield, circular rings, and the excitation source(s), accurately account for the electromagnetic interactions between the coil and the tissue. As a result, close agreement was achieved between the FDTD results and MRI images obtained at 8 Tesla.

The results show strong electromagnetic interactions between the coil in general, the excitation source(s) in particular, and the human head. As such, it is shown that the specific absorption rate (SAR) values are largely dependent on these interactions. Comparisons of linear, 2-port quadrature, and 4-port excitations with respect to SAR values were performed at 340 MHz (8 Tesla). The analysis reveals the advantages of using 4-port drive over the conventional 2-port quadrature excitation especially in reducing the SAR peak values.

1. INTRODUCTION

Studies of microwave power absorption and heating [1-3] in human tissue have shown that local hot spots often develop in tissue. These hot spots commonly occur in areas close to the source and in regions where induced current flow is restricted by surrounding low conductivity objects, e.g., in the joints. In addition, there is a need to examine power deposition in certain small body features, including the lens of the eye, which is especially susceptible to thermal damage.

As magnetic resonance imaging (MRI) is now performed at fields in excess of 1.5 Tesla, violation of local specific absorption rate (SAR) FDA limits (8 watts/Kg in any gram over the head in a 5 minute exposure, taken from the web page of the FDA: *www.fda.gov/cdrh/ode/magdev*) can become a major concern. Nonetheless, accurate SAR prediction in these small regions requires a detailed model of the tissue. In addition, at high field strength, the RF coil performance, including efficiency, and the homogeneity of the transverse magnetic field (B_1) field, is dominated by the presence of the human body and its interactions with the RF coil.

As the static magnetic (B_0) field of MRI scanners increases, the larger the ratio of the aligned nuclei in the human body becomes. Consequently, this leads to MRI images with much greater detail, which would help many diagnostic applications including early detection of tumors. However on the technical side, the Larmor frequency (the spin precession frequency of Hydrogen) rises linearly with increasing B_0 field. As such, the operational frequency for proton imaging rises to equal the Larmor frequency. As a result of the increase of the operational frequency, the applied RF field wavelength in tissue becomes smaller and the electrical dimensions of the RF coil and the large anatomical structures of the head/body become comparable.

For instance, at 8 Tesla, the operational frequency for proton

imaging is 340 MHz. The wavelength inside the head (average dielectric constant of 64) is approximately 11 cm. Therefore, the distance between back and front of the head is about twice the operational wavelength. Given this fact and that the human head is asymmetrical and contains highly inhomogeneous lossy materials, very strong electromagnetic interactions are expected between the RF coil, the excitation source(s) and the tissue. This can result in non-useful images, since the distribution of the circularly polarized component of the applied transverse magnetic (B_1) field is now prone to be inhomogeneous in the human head. The interactions between the coil, excitation source(s) and the tissue can also lead to undesired local hot spots in certain organs. Therefore, an accurate model of the tissue is a necessity for studying the aforementioned topics.

An anatomically detailed human head mesh was developed from MRI images. The high-resolution $(2\ mm)^3$ 18-tissue head model was used to provide SAR calculations inside the human head at ultra high field MRI (8 Tesla, 340 MHz). The calculations were done in the TEM resonator [4-7], a commonly used RF coil for high field MRI, with the finite difference time domain (FDTD) [8] method. The FDTD representation accurately models the coil structure including the coaxial rods, the shield, the top and bottom rings, and the excitation source(s). More importantly, the coil and the head are modeled together as a single system, which accounts for all the coupling effects between the TEM resonator and the human head. This includes the interactions between the coil, excitation source, and the head. It will be demonstrated that the number and the location(s) of the excitation port(s) significantly affect the SAR values at 340 MHz.

2. THE HUMAN HEAD MODEL

Recently, The Ohio State University has developed an anatomically detailed human head mesh. The mesh data was obtained from 0.5 mm * 0.5 mm * 2 mm MRI images; therefore, it is suitable for these types of MRI calculations. The tissue types in each image were determined and encoded on a digital image. A sample of the MRI images (a) and its encoded digital image (b) appear in Figure 1 [9].

To obtain an accurate detail of the internal human head structure, eighteen different tissue types, in addition to air, were identified in the images. By having 18 different tissue types and a small pixel size, one can obtain very accurate results especially in modeling the internal electromagnetic fields within the biological tissues, which greatly affect the SAR calculations and the B_1 field distribution in the human head. The identified tissue types are given as follow: blood, bone-cancellous, bone-cortical, cartilage, cerebellum, cornea, cerebro spinal fluid (CSF), dura, fat, gray-matter (GM), mucosa, muscle, nerve, skin, tongue, vitreous-humor, white-matter (WM), and mixed-GM-WM.

The electrical constitutive parameters of these tissues are dispersive. Thus, in any particular simulation, one must use the conductivity and the dielectric constant associated with the frequency of interest. This is done by tuning the coil to the frequency of interest and simultaneously using the constitutive parameters associated with this particular frequency. The density ρ, and dielectric constant ε_r, and the conductivity σ for these tissue types were obtained at 340 MHz [10].

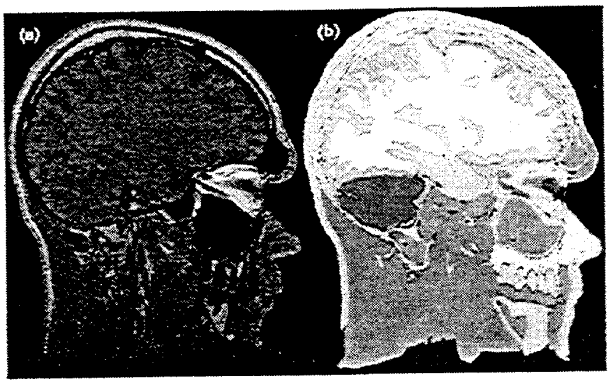

Figure 1. An MRI image (a) and its equivalent data slice (b) from the new anatomically detailed human head model.

3. THE TEM RESONATOR IN THE FDTD GRID

In Figure 2, a photograph of the transverse electromagnetic (TEM) resonator is displayed. The coil consists of 16 struts, which are contained in an open resonant cavity. Two circular rings are attached to the top and bottom of the open cavity. Each of the struts consists of coaxial line with a circular cross section. Teflon is used as a dielectric filler between the inner and outer rods of each strut. The coil is tuned by adjusting the gap between the two inner rods of each strut. In the experimental settings, this operation is done while the sample is loaded in the coil.

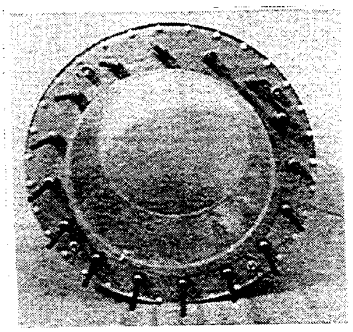

Figure 2. Photograph of a 16-strut TEM resonator used for human head imaging at 8 Tesla.

The dimensions of the Yee cells were chosen to be $(2\ mm)^3$ to fully characterize the structure of the coil including the coaxial rods and the excitation source. A stair step approximation was chosen to characterize the curved shape of the shield and the upper and lower rings of the coil. The coaxial rods were modeled in a similar manner while an FDTD algorithm was used to account for the curvatures of the rods to minimize the error caused by stair-stepping. The FDTD algorithm treats the 2-D 45° slanted cells by applying Stokes Theorem over the triangular area of interest. The largest side of the triangle constitutes a PEC. Figure 3 shows an FDTD grid of the three-dimensional structure along with axial, sagittal, and coronal slices of a 16-strut TEM resonator loaded with the anatomically detailed human head model.

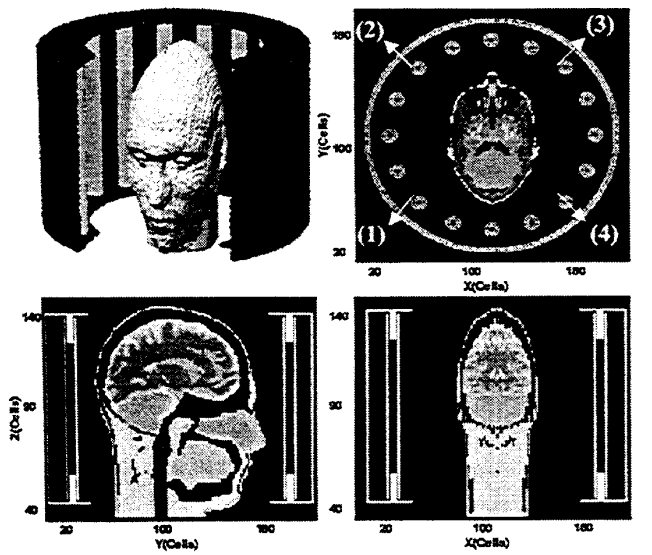

Figure 3. Three-dimensional structure and axial, sagittal, and coronal slices of a 16-strut TEM resonator loaded with the 18-tissue anatomically detailed human head model in the FDTD grid. The cells represent FDTD Yee cells.

The perfectly matched layer (PML) absorbing boundary conditions [11] were used to account for RF radiation from the coil. 16 PML cells were used on the top and bottom of the circular cavity with at least 10 free space cells separation between the PML surface and the closest cell(s) on the system (coil and human head). The systems closest spatial regions to the PML surface are coil geometry in the case of the upper circular ring or the neck of the human head (Figure 3 top-left quarter). 8 PML cells were used around the cavity of the coil with at least 2 free space cell separation between the PML surface and the closest point on the cavity. The PML cells had quadratic electric and magnetic conductivity profiles where the maximum conductivity is 1.0 S/m.

The grid had $(2\ mm)^3$ resolution resulting in a total of 8 million cells. Excluding the unknowns created by the PML split equations; the code required the calculations of 48 million time domain unknowns and 48*2 million frequency domain unknowns (real and imaginary components). The time step size was set to 3.75 ps.

To obtain the field distribution within the coil at the resonance frequency, the coil has to be numerically tuned. First a relative dielectric constant of 2.2, which is equal to that of Teflon used in the experimental coil, was assigned to the filler between the inner and the outer rods of each strut. Numerical tuning is achieved by adjusting the size of the gap between the inner rods of each strut so that the resonance frequency of mode 1 (mode of interest) matches the Larmor frequency.

In order to generate the field distribution, a two-step process was utilized. In the first step, an initial guess was made for the size of the gap between the two inner rods of each of the struts. The Fast Fourier Transform (FFT) was then applied to the FDTD solution at a few points within the grid to obtain the frequency response at those points. If the resonance frequency of the solution was not at the desired value, then the gap size was changed, and the FDTD program was re-applied. This step was repeated until the desired resonance frequency was obtained. Figure 4. shows a frequency response of one point inside the anatomically detailed human head model loaded in a 16-strut TEM resonator. Nine resonances are observed due to the fact that an N-strut TEM resonator has N/2 +1 TEM modes. Theoretically the aforementioned modes are not considered to be transverse electromagnetic (TEM) since the coil is operating at high frequency and is loaded with a lossy and a highly inhomogeneous object.

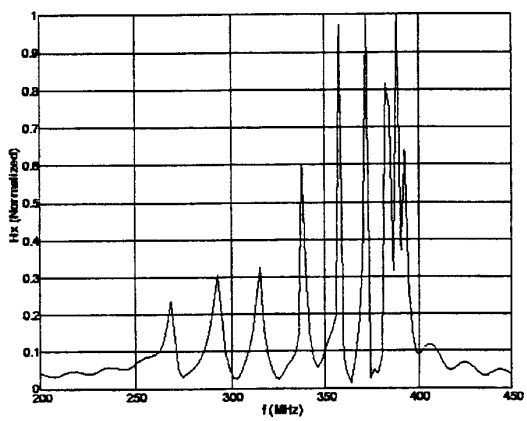

Figure 4. Frequency response of one point inside the anatomically detailed head model loaded in a 16-strut TEM

resonator. The results are calculated using the FDTD model where the coil is numerically tuned to 340 MHz (8 Tesla).

In the second step, the FDTD solution was obtained with the correct gap size, but instead of applying the FFT at a few points in the grid, a Discrete Fourier Transform was applied on-the-fly at all the points in the grid at the resonant frequency. Thus, the time data does not need to be stored, and at the end of the computer run, the field distribution is known at the resonant frequency. Classically, from the magnetic and electric field distributions, one can extract the B_1 field, SAR, the total power absorbed by the tissue, and power radiated by the coil. Note that the RF coil and the human head were modeled as a single system in the FDTD representation. This was done in all the steps of the model including, numerical tuning, and excitation. Only the single system technique allows us to accurately analyze issues such the local effect of the excitation source(s) on SAR and how the load affects the currents on the coil struts.

4. EXPERIMENTAL VALIDATION

To validate the simulations, images were acquired on the 8 Tesla/80 cm bore superconducting magnet at The Ohio State University. Low flip angle gradient echo images of a volunteer were acquired using a 16-strut TEM resonator. The experiment utilized 2-port quadrature excitation where 0 and $\pi/2$ phase shifts were applied on the excitation ports. The two drive ports were spatially positioned behind the head, and 90° apart with respect to the imaginary circle that contains the coaxial lines.

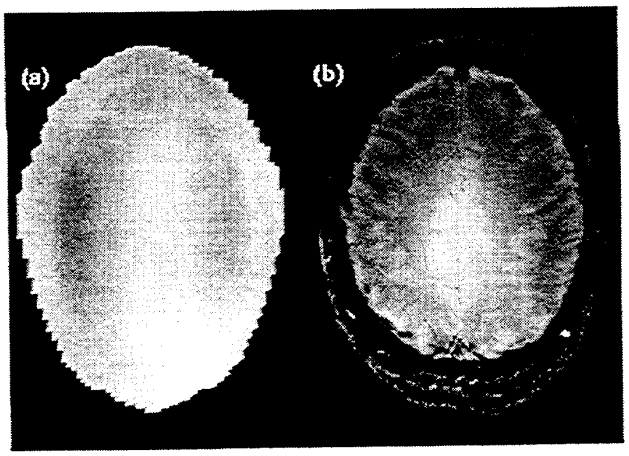

Figure 5. Axial slices of the calculated circularly polarized component of the B_1 field (a) and of a low flip angle gradient echo image (b). The results are obtained using 16-strut TEM resonator with back of the head 2-port quadrature excitation at 8 Tesla (340 MHz). The mathematical model of the coil used in the simulations had the same size and geometry as the coil used in experiment.

A simulation of a 16-strut TEM resonator loaded with the human head model was also performed at 340 MHz. The mathematical model of the coil had the same geometry and dimensions as the coil used in the actual MRI experiment. The model used 2-port quadrature excitation where the drive ports were positioned behind the head (# 1 and 4 in Figure 3). Figure 5 displays an axial slice of the calculated circularly polarized component of the B_1 field using the FDTD Model at 340 MHz (a) and of the low flip angle gradient echo image obtained at 8 Tesla (b). It is apparent that the shading and brightness of the MRI image are similar to the field distribution obtained using the FDTD model.

5. SPECIFIC ABSORPTION RATE CALCULATIONS AT 340 MHz (8 TESLA)

An important aspect of RF coil design for magnetic resonance imaging applications is RF power absorption by the patient. Furthermore, the critical health concern is not RF power deposition but the rise in temperature that it produces. In practice, the most important concerns are the ``hot spots" produced by small-scale tissue features.

Fields within the body are difficult to estimate accurately because of their dependence on the body's complicated internal structure. Therefore, high resolution anatomically detailed human head/body models are essential to describe specific absorption rate (SAR) in general, and local SAR maximas (hot spots) in particular for high frequency MRI applications.

Classically, the SAR is given by

$$SAR = \frac{1}{2\rho}\sigma\left|\vec{E}\right|^2 \qquad (1)$$

where σ *(S/m)* and ρ *(Kg/m^3)* are the conductivity and the mass density of the tissue, respectively. $\left|\vec{E}\right|$ *(V/m)* is the magnitude of the electric field in the tissue. By evaluating the SAR within specific tissues, one can obtain the power deposition for specific organs. Also, by summing the SAR from all tissues, an indication of the total power deposition and average SAR can be obtained. The SAR in the above equation is normalized to the power transmitted from the coil.

The real input power of the coil is defined as:

$$P_{IN} = P_{ABS} + P_{RAD} \qquad (2)$$

$$= \frac{1}{2}\iiint_v \sigma\left|\vec{E}\right|^2 dv + \frac{1}{2} real\{\oiint_s \vec{E}\times\vec{H}^* \bullet ds\} \qquad (3)$$

where P_{ABS} and P_{RAD} are defined as the absorbed and radiated

power, respectively while, $\iiint_V$ is the volume integral of the object to be image and $\oiint_S$ is the integral of a closed surface that encloses the coil structure and the imaged object. The volume integration is done by numerically integrating $\sigma|\vec{E}|^2$ over the human head model. The surface integration is done by first choosing a surface that encloses the coil and the sample. In this case it consists of a rectangular box which faces lie in the middle of the free space areas between the PML surface and the system (coil and the head). Numerical integration of $\vec{E}\times\vec{H}^*$ is then performed over that surface.

The following calculations are presented for 1 Watt continuos power input power. This is equivalent to a square pulse that has a 100-Watt peak power, 5 ms width, and 500 ms time recovery (TR). Three excitations are considered: linear, 2-port quadrature, and 4-port quadrature. The 2-port excitation employs 0 and $\pi/2$ phase shifts on the drive points, while the 4-port excitation utilizes 0, $\pi/2$, π, and $3\pi/2$ phase shifts. The drive ports identification numbers are displayed in the top-right quarter of Figure 3. X or Y linear excitation represents driving the coil in port 1 (X) or 2 (Y), respectively. Back, side, or front of the head 2-port quadrature excitation represents driving the coil in ports 1 and 4 (back), 1 and 2 (side), or 2 and 3 (front), respectively. 4-port quadrature excitation utilizes ports 1 to 4.

Figure 6 displays axial slices of the SAR distribution calculated inside the human head model using 16-strut TEM resonator tuned to 340 MHz. Note that each subfigure of Figure 6 has its own gray scale with its unique minimum and maximum values. The grays scale however is still linear. Figures 6a and 6b correspond to X (a) and Y (b) linear excitation. Figures 6c, 6d, and 6e correspond to 2-port quadrature drives using back (c), front (d), and side (e) of the head excitation locations. Figure 6f displays the SAR distribution for 4-port quadrature excitation.

Figures 6a and 6b show that the SAR increases in the areas near the rods through which relatively high absolute values of currents are flowing. Figure 3 shows that X linear excitation utilizes rod 1 as a drive point. As such, the two rods, which are expected to carry the maximum amount of current, are 1 and 3, while rods 2 and 4 are expected to have minimal amount of currents flowing through them. Therefore, the areas with relatively high SAR values include the top right and bottom left of the axial slice shown in Figure 6a. In the case of Y linear excitation, the peak values of the SAR are largely concentrated in the bottom right and top left of the axial slice shown in Figure 6b. The absolute values of the currents on the rods between the struts that carry maximum currents and the struts that carry minimum currents progressively decrease. At low frequency, current values on the coil struts follow a sinusoidal distribution. This is not the case at 340 MHz.

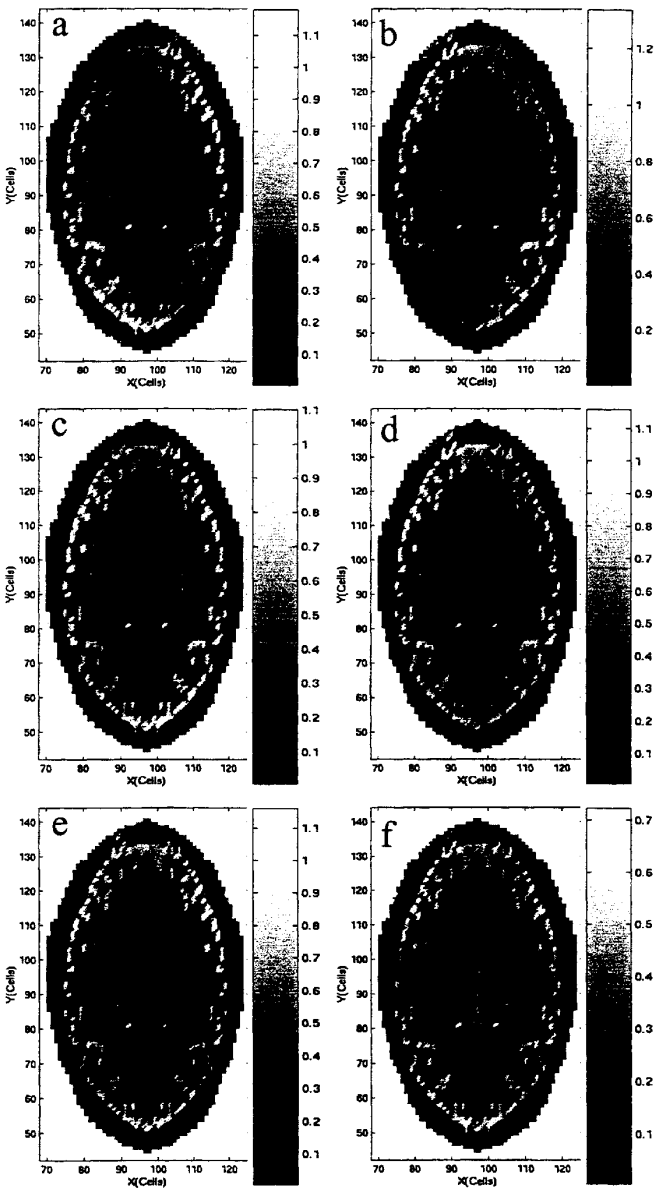

Figure 6. Axial slices of the SAR distribution inside the anatomically detailed human head model at 340 MHz. The results are obtained using the FDTD model and utilizing 16-strut TEM resonator operating under X (a) and Y (b) linear excitations, back (c), front (d), and side (e) of the head 2-port quadrature excitation, and 4-port (f) excitation. The transmitted power to the coil is equal to 1 Watt CW: a square pulse with a 100 Watt peak power, 5 ms width, and 500 ms time recovery.

The calculations show that the SAR peak values do not significantly change from linear to 2-port quadrature excitation (Figure 6 a-e). This confirms the finding [12] that at high frequency, the conventional 2-port quadrature excitation does not effectively produce circularly polarized fields. Compared to linear excitation, the input power does not significantly decrease when using 2-port quadrature excitation. This is not the case at low frequency. For instance, with the commonly used 1.5 Tesla clinical magnets where the operating frequency for proton imaging is 64 MHz, images obtained using 2-port quadrature drive usually require half of the power used in linear excitation. At 8 Tesla (340 MHz), the interactions between the coil, excitation source and the head are significant. As such, linear excitation does not produce fields which are transverse electromagnetic or linearly polarized. This results in the ineffectiveness of the conventional 2-port quadrature excitation.

When using 4-port excitation (Figure 6f) however, the coil-tissue interactions are reduced which results in a noticeable decrease in the SAR peak values. Figure 6f shows that the SAR peak values have decreased by approx. 40 % using the 4-port drive compared to the values obtained with 2-port quadrature excitations (Figures 6 b-d). The 4-port excitation distributes the energy among the struts more effectively than the conventional 2-port quadrature drive, which consequently leads to lower SAR peak values.

To study the electromagnetic interactions between the excitation source (s) and the human head, Figure 7 displays sagittal slices of the SAR values at 340 MHz. Similar to Figure 6, each subfigure of Figure 7 has its own gray scale. The results are obtained using 16-strut TEM resonator operating under X (a) and Y (b) linear, back (c), front (d), and side (e) of the head 2-port quadrature, and 4-port (f) excitations. Due to the localization and the irregular shape of the nose, strong electromagnetic interactions are expected between this structure and the coil in general or the excitation source(s) in particular. This is demonstrated in Figure 7b where the SAR peak values are observed in the nose. In this case (Y linear drive), the excitation source is close to the nose resulting in higher SAR peak values compared to the case where X linear drive (7a) is utilized.

The 2-port quadrature excitations reveal similar results (Figures 7c-e). SAR peak values concentrated in the nose significantly increase from back (7c), 2 drive ports are furthest from the nose, to side (7e), 1 drive port is closest to the nose, to front (7d), 2 drive ports are closest to the nose, of the head quadrature excitation. The 4-port excitation (7f) displays similar results except the SAR peak values in the nose are less than those obtained with Y linear excitation (7b) or with front of the head (7d) quadrature excitation. As previously stated, 4-port drive effectively distributes the energy among the struts. As a result, lower SAR peak values are observed compared to linear and 2-port excitations.

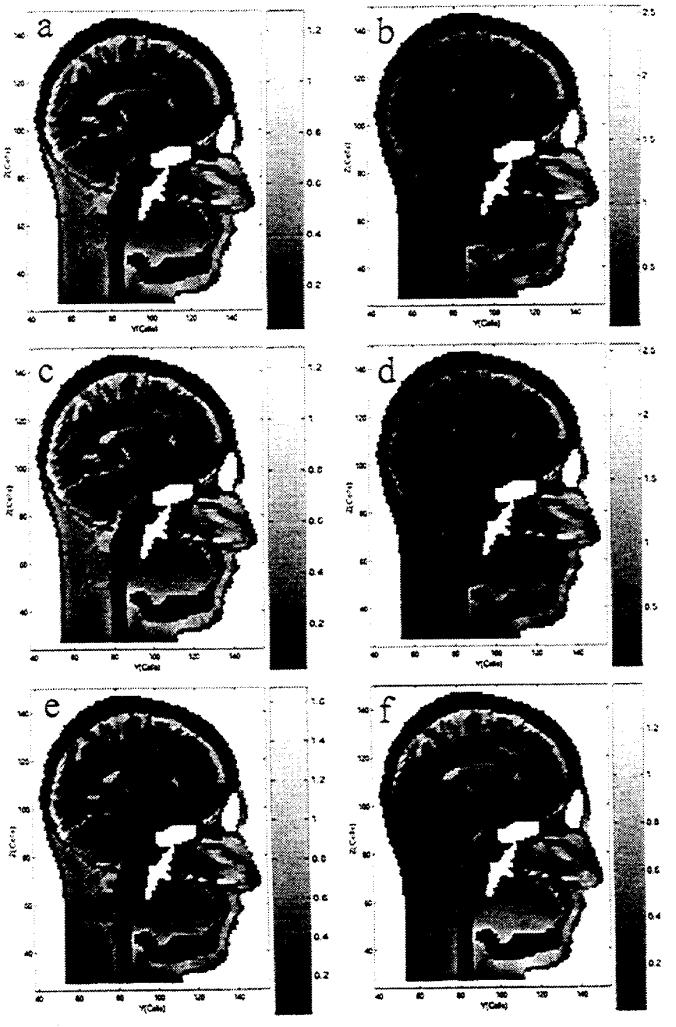

Figure 7. Sagittal slices of the SAR distribution inside the anatomically detailed human head model at 340 MHz. The results are obtained using the FDTD model and utilizing 16-strut TEM resonator operating under X (a) and Y (b) linear excitations, back (c), front (d), and side (e) of the head 2-port quadrature excitation, and 4-port (f) excitation. The transmitted power to the coil is equal to 1 Watt CW.

6. CONCLUSIONS

In this work, a complete electromagnetic analysis of the TEM resonator, an RF coil used for high frequency magnetic resonance imaging applications, is presented at 340 MHz (8 Tesla). The study of the RF coil is performed using the finite difference time domain (FDTD) method. A (2 mm)^3

anatomically detailed human head model was developed and utilized in the FDTD study of the TEM resonator. The coil and the head were modeled together as a single system. Therefore, the FDTD analysis accounts for the electromagnetic coupling between the coil, excitation source(s), and the human head. The FDTD calculated circularly polarized component of the transverse magnetic (B_1) field was in close agreement with low flip angle gradient echo human head images obtained at 8 Tesla.
The coil was numerically tuned to 340 MHz, where classical specific absorption rate (SAR) calculations were done inside the human head model. The FDTD results of the SAR distribution in axial slices through the brain, indicate that the peak values of the SAR is greatly reduced when switching from linear or 2-port quadrature drives to 4-port excitation. In addition, the FDTD simulations also show that the SAR peak values are affected by the excitation source(s) and their location(s). Thus, for high frequency MRI applications, it is necessary to properly model the physical excitation source(s) of the coil rather than assume a current distribution on the coil struts in order to explain the electromagnetic phenomena.

7. ACKNOWLEDGEMENTS

The Compaq Dec at the Aeronautical Systems Command Major Shared Resource Center of the Wright Patterson Air Force Base was used to generate the numerical results.

8. REFRENCES

1. Chen J-Y, Gandhi OP. Numerical Simulation of annular-phased arrays of dipoles for hyperthermia of deep-seated tumors. *IEEE Trans. Biomed. Eng.* **39**:209-216; 1992.

2. Lynch DR, Paulsen KD, Strohbehn JW. Finite element solution of Maxwell's equations for hyperthermia treatment planning. *J Comp. Phy.* **58**:246-269; 1990.

3. Wang C-O, Gandhi OP. Numerical simulation of annular phased arrays for anatomically based models using the FDTD method. *IEEE Trans. Micro. The. Tech.* **37**:118-126; 1989.

4. Roschmann PK. High-Frequency Coil System for Magnetic Resonance Imaging Apparatus. U.S. Patent 4746866; 1988.

5. Vaughan JT, Hetherington HP, Otu JO, Pan JW, Pohost JM. High frequency volume coils for clinical NMR imaging and spectroscopy. *Magn. Reson. Med.* **32**:206-218; 1994.

6. Robitaille P-ML. Black body and transverse electromagnetic resonators operating at 340 MHz: Volume RF coils for ultra high field MRI. *J. Comp. Assist. Tomogr.* **23**:879-890; 1999.

7. Baertlein BA, Ozbay O, Ibrahim TS, Lee R, Kangarlu A, Robitaille P-ML. Theoretical model for an MRI radio frequency resonator. *IEEE Trans. Biomed. Eng.* **47**:535-546; 2000.

8. Yee KS. Numerical solution of initial boundary value problems involving Maxwell's equations in isotropic media. *IEEE Trans. Ant. Prop.* **AP-14**:302-307; 1966.

9. Ibrahim TS, Lee R, Baertlein BA, Kangarlu A, Robitaille P-ML. Effect of RF coil excitation on field inhomogeneity at ultra high fields: A field optimized TEM resonator. *Magn. Reson. Imag.* Submitted for publications.

10. Gabriel C. Compilation of dielectric properties of body tissues at RF and microwave frequencies. *AL/OE-TR-1996-0037*; 1996.

11. Berenger J. A perfectly matched layer for the absorption of electromagnetic waves. *Computational Phy.* **114**:185-2000; 1994.

12. Ibrahim TS, Lee R, Baertlein BA, Kangarlu A, Robitaille P-ML. Application of finite difference time domain method for the design of birdcage RF head coils using multi-port excitations. *Magn. Reson. Imag.* **18**:733-742; 2000.